

九州工業大学学術機関リポジトリ



Title	Staggered Local Density of States around the Vortex in Underdoped Cuprates
Author(s)	Kishine, Jun-ichiro; Lee, Patrick A; Wen, Xiao-Gang
Issue Date	2001-06
URL	http://hdl.handle.net/10228/666
Rights	Copyright © 2001 American Physical Society

Staggered Local Density of States around the Vortex in Underdoped Cuprates

Jun-ichiro Kishine,* Patrick A. Lee, and Xiao-Gang Wen

Department of Physics, Massachusetts Institute of Technology, Cambridge, Massachusetts 02139

(Received 7 March 2001)

We have studied a single vortex with the staggered flux (SF) core based on the SU(2) slave-boson theory of high T_c superconductors. We find that, whereas the center in the vortex core is a SF state, as one moves away from the core center a correlated staggered modulation of the hopping amplitude χ and pairing amplitude Δ becomes predominant. We predict that in this region the local density of states exhibits staggered modulation when measured on the bonds, which may be directly detected by STM experiments.

DOI: 10.1103/PhysRevLett.86.5365

PACS numbers: 74.25.Jb, 71.10.Fd, 71.27.+a

The elucidation of the ground state properties of the high T_c cuprates has been one of the major challenges in condensed matter physics. Recent STM experiments on vortices [1,2] have indicated the existence of a normal core with a gap structure characteristic of the normal state pseudogap above T_c . The theoretical description of the normal core, however, remains unresolved [3–5]. Based on the SU(2) slave-boson theory of the high T_c superconductors [6,7], Lee and Wen [8] proposed a model of the vortex with a staggered flux (SF) core, characterized by a pseudogap and staggered orbital current. The signature of the SF order in zero field was found in the Gutzwiller-projected d -wave superconducting state by a variational Monte Carlo method [9] and exact diagonalization of the t - J model [10]. By using a Gutzwiller-projected U(1) slave-boson mean-field wave function, Han and co-workers recently found evidence of the SF order near the vortex core [11,12]. The natural question arises as to whether the SF core has observable consequences for the tunneling spectra using atomic resolution STM. This is the question addressed by this Letter.

We first summarize some of the salient feature of the SU(2) vortex structure. In the SU(2) slave-boson theory [6], the physical electron is represented by a spin-1/2 fermion operator $f_{i\sigma}$ and a charge-1 boson operator $h_i^T = (b_{i1}, b_{i2})$: $c_{i\sigma} = \frac{1}{\sqrt{2}} h_i^\dagger \psi_{i\sigma}$, where h_i and $\psi_{i\sigma}^T = (f_{i\sigma}, \varepsilon_{\sigma\bar{\sigma}} f_{i\bar{\sigma}})$ are SU(2) doublets. The slave-boson mean-field state is characterized by 2×2 matrices $U_{ij} = \begin{pmatrix} -\chi_{ij} & \Delta_{ij} \\ \Delta_{ij}^* & \chi_{ij} \end{pmatrix}$ on the links and boson condensation h_i on the sites. The U_{ij} describe the hopping of the fermions and bosons. The mean-field solution is obtained by integrating out the fermions and minimizing the mean-field energy $E(\{U_{ij}, h_i\})$, which leads to $\chi_{ij} = \langle f_{i\sigma}^\dagger f_{j\sigma} \rangle$ and $\Delta_{ij} = \langle \varepsilon_{\sigma\bar{\sigma}} f_{i\sigma} f_{j\bar{\sigma}} \rangle$. The SU(2) gauge invariance is realized through the relation $E(\{U_{ij}, h_i\}) = E(\{W_i U_{ij} W_j^\dagger, W_i h_i\})$, for any $W_i \in \text{SU}(2)$. In the underdoped region, the mean-field solution has the following form (in the SF gauge): $U_{ij}^{\text{SF}} = -A\tau^3 \exp[i(-1)^{i_x+j_y} \Phi_0 \tau^3] \exp[-ia_{ij}^3 \tau^3]$ with $A = \sqrt{\chi^2 + \Delta^2}$ and $\Phi_0 = \tan^{-1}(\Delta/\chi)$. This describes fermions hopping with flux $\pm 4\Phi_0$ on alternating plaquettes [13]. The

advantage of the SF gauge is that it is apparent that the SU(2) symmetry has been broken down to the residual U(1), since U_{ij}^{SF} contains only τ^3 . As a result, the low lying fluctuations have a simple form in the SF gauge:

$$\bar{U}_{ij}^{\text{SF}} = -A\tau^3 \exp[i(-1)^{i_x+j_y} \Phi_0 \tau^3] \exp[-ia_{ij}^3 \tau^3]. \quad (1)$$

These fluctuations are described by the lattice gauge field a_{ij}^3 .

In the presence of a magnetic field, the mean-field solution contains vortices. Since the bosons are locally condensed to the bottom of the band, they can be parametrized by $(\bar{h}_i^{\text{SF}})^T = \sqrt{x}(z_{i1}, -i(-1)^{i_x+i_y} z_{i2})$, where z_{i1} and z_{i2} are slowly varying in space and time. The vortex is now described by the twisted z_i field and U_{ij} in Eq. (1). To write down the vortex structure explicitly, let us introduce $z_{i1} = e^{i\varphi_{i1}} \cos \frac{\theta_i}{2}$ and $z_{i2} = e^{i\varphi_{i2}} \sin \frac{\theta_i}{2}$, where $\varphi_{i1} = \alpha_i - \phi_i/2$ and $\varphi_{i2} = \alpha_i + \phi_i/2$. The phase angles α_i and ϕ_i are associated with the electromagnetic (EM) U(1) and the a^3 U(1) gauge structures, respectively. The internal degrees of freedom ϕ and θ can be visualized by the vector $\mathbf{I}_i = z_i^\dagger \boldsymbol{\tau} z_i = (\sin\theta_i \sin\phi_i, -\sin\theta_i \cos\phi_i, \cos\theta_i)$, which has the meaning of the quantization axis for the z_i fields.

In the vortex structure proposed by Lee and Wen [8], both α_i and $\phi_i/2$ wind by π and consequently give an appropriate $hc/2e$ vortex for the EM gauge field $\mathbf{A}(\mathbf{r})$, i.e., $\nabla\alpha = \nabla\phi/2 = \hat{\mathbf{e}}_\phi/2r$ which leads to $\nabla\varphi_1 = 0$ and $\nabla\varphi_2 = \hat{\mathbf{e}}_\phi/r$, where $\hat{\mathbf{e}}_\phi$ denotes the azimuthal unit vector in the physical space. That is to say, only b_2 changes its phase φ_2 by 2π as we go around the vortex, while b_1 does not. Outside the vortex core, $\mathbf{I}_i = (\sin\phi_i, -\cos\phi_i, 0)$ [see Fig. 1(a)], which describes a d -wave superconducting state. As we approach the core, $|b_2|$ must vanish and the vortex center is represented by $\mathbf{I}_i = (0, 0, 1)$, which is just the metallic SF state. The \mathbf{I}_i vector tilts smoothly from the equator to the north pole as the core is approached with a length scale denoted by ℓ_c . At the same time, the gauge flux $\mathbf{h} = \nabla \times \mathbf{a}^3$ is distributed over a distance scale of λ_a and it is expected that $\lambda_a \sim x^{-1} \geq \ell_c$. Inside λ_a , the gauge invariant combination

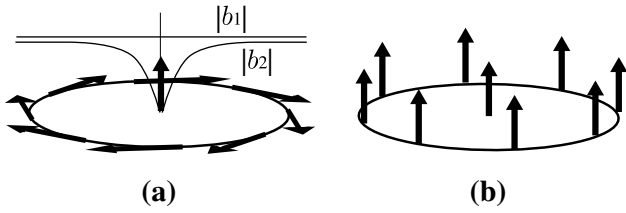


FIG. 1. (a) Configuration of the I_i vector outside the SF core in the SF gauge. At the center of the vortex, $I_i = z_i^\dagger \tau z_i = (\sin\theta_i \sin\phi_i, -\sin\theta_i \cos\phi_i, \cos\theta_i)_i$ points toward the north pole, which corresponds to the SF state. The local gauge transformation g_i transforms this configuration to (b) in the d -wave gauge, where the internal phases of the Bose condensate are gauged away.

$$\mathcal{V}_{ij} = \frac{\phi_i - \phi_j}{2} - a_{ij}^3 \quad (2)$$

and its continuum limit, $\mathcal{V}(\mathbf{r}) = \frac{1}{2} \nabla \phi(\mathbf{r}) - \mathbf{a}^3(\mathbf{r})$, is finite. This is the analog of the superfluid velocity inside the London penetration depth λ_L in conventional vortices, except that here $\lambda_a \ll \lambda_L$ and the effect of the EM field A is negligible.

The physics of the local electronic state is better visualized by making a local gauge transformation $\psi_{i\sigma} \rightarrow g_i \psi_{i\sigma}$, $\bar{U}_{ij}^{\text{SF}} \rightarrow g_i \bar{U}_{ij}^{\text{SF}} g_j^\dagger$, and $(\bar{h}_i^{\text{SF}})^T \rightarrow (g_i \bar{h}_i^{\text{SF}})^T = e^{i\alpha_i}(\sqrt{x}, 0)$, i.e., the local boson isospin vector points toward the north pole, as shown in Fig. 1(b). The explicit g_i is given by $g_i = \exp[i(-1)^{i_x+i_y} \frac{\theta_i}{2} \tau^1] \exp[i \frac{\phi_i}{2} \tau^3]$. The advantage of this gauge is that the physical electron operator $c_\sigma \propto f_\sigma$. The new U_{ij} has a physical meaning as governing the hopping and pairing of electrons. We shall refer to this as the d -wave gauge. Indeed, locally there is a single boson component and the problem reduces to the more familiar U(1) mean-field theory, but with χ_{ij} and Δ_{ij} which vary in space. This is precisely the problem treated by Han and co-workers [11,12] and it is gratifying that they found numerically the staggered current around the vortex core, as proposed in Ref. [8].

Now we are ready to ask the question: Is any signature of the unit cell doubling directly measurable by STM tunneling? It turns out that there is no effect in the SF phase in the center of the core, because the period doubling of the *current* does not show up in the local density of states (LDOS). This leads us to look outside the immediate core and examine the effect of the phase winding, i.e., the effect of \mathcal{V}_{ij} . After a local gauge transformation to the d -wave gauge, we find that Eq. (1) becomes

$$\begin{aligned} \bar{U}_{ij}^d = & -\chi_{ij} \left(\tau^3 \cos \frac{\theta_i - \theta_j}{2} + \tau^2 \sin \frac{\theta_i - \theta_j}{2} \right) \\ & - \Delta_{ij} \left[i(-1)^{i_x+j_y} \cos \frac{\theta_i + \theta_j}{2} \right. \\ & \left. - (-1)^{i_y+j_y} \tau^1 \sin \frac{\theta_i + \theta_j}{2} \right], \quad (3) \end{aligned}$$

where

$$\chi_{ij} = A \cos \Phi_{ij}, \quad \Delta_{ij} = A \sin \Phi_{ij}, \quad (4)$$

and

$$\Phi_{ij} = \Phi_0 + (-1)^{i_x+j_y} \mathcal{V}_{ij}. \quad (5)$$

We now interpret this equation in different limits. First, we consider the region far outside the SF core. In this region, $\theta_i \sim \theta_j \sim \pi/2$ and Eq. (3) becomes $\bar{U}_{ij}^d \sim -\chi_{ij} \tau^3 + (-1)^{i_y+j_y} \Delta_{ij} \tau^1$. Recalling that χ_{ij} and Δ_{ij} are interpreted as the hopping and pairing amplitudes of physical electrons, we see that *the region outside the SF core is characterized by the staggered amplitude modulation*. Note from Eq. (4) that the amplitude of χ_{ij} and Δ_{ij} is modulated in a correlated way to preserve $\chi_{ij}^2 + \Delta_{ij}^2 = \text{const}$. In Fig. 2, we schematically show the modulation pattern of χ_{ij} . In this region, \bar{U}_{ij}^d breaks the translational symmetry, but does not break the time reversal symmetry.

Second, we consider the vicinity of the vortex center, where $\theta_i \sim \theta_j \sim 0$ and Eq. (3) becomes $\bar{U}_{ij}^d \sim -A \tau^3 \exp[i(-1)^{i_x+j_y} \Phi_{ij} \tau^3]$. In this region, \bar{U}_{ij}^d breaks both the translational and the time reversal symmetries, and the staggered orbital current appears [8]. However, the staggered flux is further modulated according to Eq. (5).

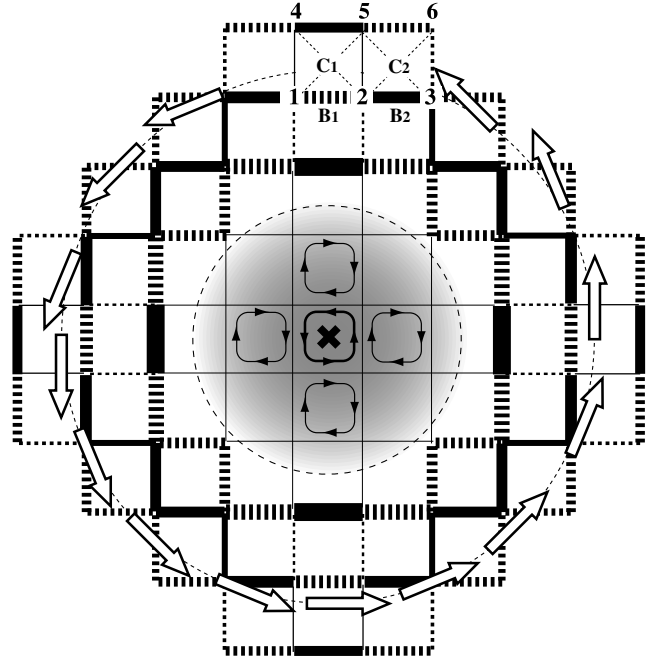


FIG. 2. Schematic drawing of the amplitude modulation pattern of the hopping field χ_{ij} outside the SF core. Solid and dotted bonds indicate enhanced and reduced amplitudes, respectively, where the thickness of the bonds qualitatively represents the magnitude of the modulation. Circulation of the field, $\mathcal{V}(\mathbf{r})$, is indicated by the arrows. The dotted circle represents the SF core boundary, $r = \ell_c$, inside which the staggered orbital current flows. Note that the boundary should not be taken literally. In reality, there is a crossover region around $r \sim \ell_c$, where the staggered current and the staggered amplitude modulation coexist.

As we approach the core from the outside, the \mathbf{I}_i vector in the SF gauge representation gradually rises from the equatorial plane [see Fig. 1(a)]. This gives rise to a crossover region characterized by the coexistence of the amplitude and phase modulations, where the θ dependence of \bar{U}_{ij}^d becomes significant. However, to study the effects of a θ -dependent \bar{U}_{ij}^d is beyond the scope of this paper. From now on, we shall compute the LDOS by setting $\theta_i = \theta_j = \pi/2$. We expect our results to be qualitatively valid for $r \lesssim \ell_c$ as long as we avoid the exact core center.

The presence of staggered modulation of χ_{ij} and Δ_{ij} in this region suggests that this may be the best place to look for unit cell doubling effects. To model the tunneling current, we assume that the electrons tunnel from the tip, located at \mathbf{r} , to a linear combination of Wannier orbitals centered at lattice sites i , i.e., $\sum_i \alpha_i(\mathbf{r})\phi(\mathbf{r} - \mathbf{r}_i)$. Then the LDOS in the d -wave gauge is written as

$$N(\mathbf{r}, \omega) = -\frac{2x}{\pi} \text{Im} \sum_{i,j} \alpha_i(\mathbf{r})\alpha_j(\mathbf{r}) [\mathcal{G}_{ij}^F(i\omega)]_{11} |_{i\omega=\omega+i\delta}. \quad (6)$$

The subscript 11 means the 11 component of the lattice fermion propagator in a 2×2 matrix form, $\mathcal{G}_{ij}^F(i\omega) = -\int_0^\beta d\tau e^{i\omega\tau} \langle T_\tau \psi_{i\sigma}(\tau) \psi_{j\sigma}^\dagger \rangle$.

Here we demonstrate that the LDOS exhibits a conspicuous staggered pattern only when measured on the bonds. For example, we pick up the sites 1, 2, ..., 6 indicated in Fig. 2 and consider the midpoints on the bonds, B_1, B_2 , and the plaquette centers, C_1, C_2 . The LDOS at C_1 and C_2 comes from $\sum_{i,j=1,2,4,5} \mathcal{G}_{ij}^F$ and $\sum_{i,j=2,3,5,6} \mathcal{G}_{ij}^F$, respectively. We see, however, that $\mathcal{G}_{12}^F \sim \mathcal{G}_{56}^F$ since the bonds 12 and 56 are almost equivalent, except for a small inequivalence coming from the nonuniformity of the slowly-varying $\mathcal{V}(\mathbf{r})$ field. Similarly, $\mathcal{G}_{45}^F \sim \mathcal{G}_{23}^F$ and $\mathcal{G}_{14}^F \sim \mathcal{G}_{36}^F$. Therefore, $N(C_1, \omega) \sim N(C_2, \omega)$. Similarly, the LDOS

at the lattice sites is almost uniform. On the other hand, the LDOS at B_1 and B_2 comes from $\sum_{i,j=1,2} \mathcal{G}_{ij}^F$, and $\sum_{i,j=2,3} \mathcal{G}_{ij}^F$, respectively. Here, \mathcal{G}_{12}^F and \mathcal{G}_{23}^F are clearly inequivalent because they connect bonds with alternating hopping-pairing amplitudes. Furthermore, it is seen that the staggered modulation of the LDOS becomes most conspicuous when scanned along the a or b axis [see the inset of Fig. 3(a)], because on these bonds the circulating $\mathcal{V}(\mathbf{r})$ field becomes parallel to the bond directions. From now on, we shall concentrate on the LDOS at the point $\mathbf{r} = (0, i_y + 1/2)$ with lattice unit. To evaluate $\mathcal{G}_{ij}^F(i\omega)$, we shall use the following two approaches which may be complementary to each other: (I) *gradient expansion*, and (II) *uniform \mathcal{V} approximation*.

(I) *Gradient expansion*.—First, we expand Eq. (4) with respect to \mathcal{V}_{ij} up to first order, which gives $\bar{U}_{ij}^d = U_{ij}^d + \delta U_{ij}^d$ with $\delta U_{ij}^d = (-1)^{i_x+j_y} [\Delta\tau^3 + (-1)^{i_y+j_y} \chi\tau^1] \mathcal{V}_{ij}$. Second, we treat the effect of δU_{ij} within the Born approximation. In this case, we can take into account the circulating configuration of the $\mathcal{V}(\mathbf{r})$ field.

The LDOS on the bonds is written as $N(\mathbf{r}, \omega)/x\alpha^2 = \bar{N}_0(\omega) + \delta\bar{N}(\mathbf{r}, \omega)$. The uniform counterpart is given by $\bar{N}_0(\omega) = -\frac{1}{\pi} \sum_{\mathbf{k}} \cos^2 \frac{k_x}{2} \text{Im}[\mathcal{G}_0^F(\mathbf{k}, i\omega)]_{11} |_{i\omega=\omega+i\delta}$, where $\mathcal{G}_0^F(\mathbf{k}, i\omega) = U_k/(i\omega - E_k) + V_k/(i\omega + E_k)$, $U_k = \frac{1}{2}[1 + (\gamma_k\tau^3 + \eta_k\tau^1)/E_k]$, $V_k = \frac{1}{2}[1 - (\gamma_k\tau^3 + \eta_k\tau^1)/E_k]$, and $E_k = \sqrt{\gamma_k^2 + \eta_k^2}$ with $\gamma_k = -J\chi[\cos k_x + \cos k_y + \tilde{t}_2 \cos k_x \cos k_y + \tilde{t}_3(\cos 2k_x + \cos 2k_y)] + a_0$ and $\eta_k = +J\Delta(\cos k_x - \cos k_y)$. We took account of the second and third nearest neighbor hopping of the fermions [$\tilde{t}_2 = -0.550$ and $\tilde{t}_3 = 0.087$] to reproduce the real band structure of $\text{Bi}_2\text{Sr}_2\text{CaCu}_2\text{O}_{8+\delta}$ as measured by angle-resolved photoemission spectroscopy [14].

The staggered counterpart is given by

$$\delta\bar{N}(\mathbf{r}, \omega) \sim \frac{(-1)^{i_y}}{4} \mathcal{V}_x(\mathbf{r}) \sum_{\mathbf{k} \in \text{RZ}} \sin^2 k_x \times [L_k^+ \delta(\omega; E_k, E_{k+\mathbf{Q}}) + L_k^- \delta(\omega; -E_k, -E_{k+\mathbf{Q}}) + N_k^+ \delta(\omega; E_k, -E_{k+\mathbf{Q}}) + N_k^- \delta(\omega; -E_k, E_{k+\mathbf{Q}})], \quad (7)$$

where $\mathbf{r} = (0, i_y + 1/2)$, $\delta(\omega; x, y) \equiv [\delta(\omega - x) - \delta(\omega - y)]/(x - y)$, $L_k^\pm = \Delta(1 + \gamma_+ \gamma_- - \eta_+ \eta_- \pm \gamma_+ \pm \gamma_-) \pm \chi(\eta_+ + \eta_- \pm \gamma_+ \eta_- \pm \eta_+ \gamma_-)$, $N_k^\pm = \Delta(1 - \gamma_+ \gamma_- + \eta_+ \eta_- \pm \gamma_+ \mp \gamma_-) \pm \chi(\eta_+ - \eta_- \mp \gamma_+ \eta_- \mp \eta_+ \gamma_-)$, $\gamma_+ = \gamma_{k+\mathbf{Q}}/E_{k+\mathbf{Q}}$, $\gamma_- = \gamma_k/E_k$, $\eta_+ = \eta_{k+\mathbf{Q}}/E_{k+\mathbf{Q}}$, and $\eta_- = \eta_k/E_k$. Because of staggering, a fermion with \mathbf{k} in the reduced zone (RZ) is scattered to $\mathbf{k} + \mathbf{Q}$ [$\mathbf{Q} = (\pi, \pi)$] in the second zone.

In Fig. 3(a), we show the profile of $N(\mathbf{r}, \omega)/x\alpha^2$ at the points A ($0, i_y + 1/2$), B ($1/2, i_y + 1$), C ($0, i_y + 3/2$), and D ($-1/2, i_y + 1$) by choosing i_y to satisfy $\mathcal{V}_x(i_y) = 0.1$. As a rough estimate, this corresponds to a lattice position of $i_y = 4$ if $\lambda_a = 10$. We used $a_0 = 0.05\chi J$ and $\Delta/\chi = 0.2$. Numerical integration was performed by dividing the Brillouin zone into a 320×320 mesh. Note

that, at B and D , $\delta\bar{N}(\mathbf{r}, \omega)$ almost vanishes and the LDOS is just given by $\bar{N}_0(\omega)$, because $\mathcal{V}(\mathbf{r})$ becomes almost perpendicular to these bond directions. The modulation pattern at the other points can be read off from Fig. 2.

It is remarkable that, inside the overall V-shaped profile with the sharp peaks at $\tilde{\omega} \equiv \omega/\chi J = \pm 0.323$ associated with the d -wave superconducting gap, there appears additional staggered structure around $\tilde{\omega} = \pm 0.179$ and $\tilde{\omega} = 0.226$. This structure comes from resonant scattering between the fermions with \mathbf{k} and $\mathbf{k} + \mathbf{Q}$. As ω increases from zero, the energy contours $E_k = \omega$ and $E_{k+\mathbf{Q}} = \omega$ first touch on the reduced zone boundary at $\tilde{\omega} = \pm 0.179$, as indicated in Fig. 3(b), and resonance occurs. Then, at $\tilde{\omega} = \pm 0.226$, they touch again at $(\pi/2, \pi/2)$ and the second resonance occurs. The second resonance comes up

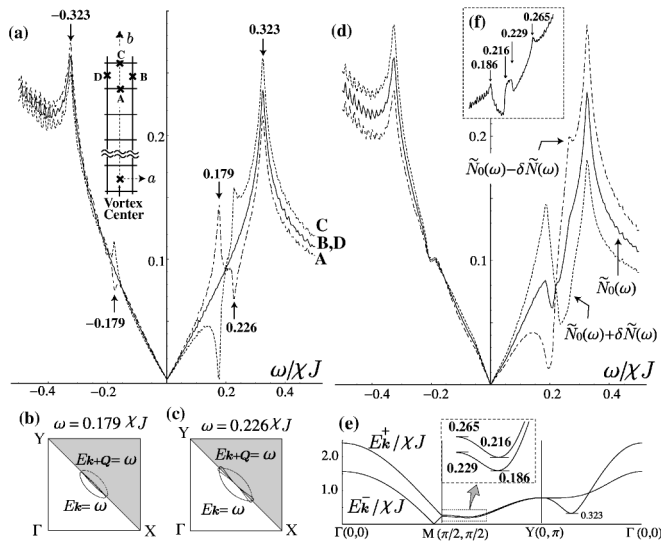


FIG. 3. (a) LDOS profile at the points A, B, C, and D indicated in the inset. The LDOS at B and C are just $\tilde{N}_0(\omega)$. The energy contours $E_k = \omega$ and $E_{k+Q} = \omega$ touch at $\tilde{\omega} = 0.179$ and $\tilde{\omega} = 0.226$, as indicated in (b) and (c), respectively. The sharp peaks at $\tilde{\omega} = \pm 0.323$ are associated with the superconducting gap. The small wiggles outside the V-shaped profile come from numerical fluctuations. (d) Profile of $\tilde{N}_0(\omega)$, and $\tilde{N}_0(\omega) \pm \delta\tilde{N}(\omega)$ for the uniform field $\mathcal{V} = (-0.1, 0)$. (e) The band dispersion of the split bands E_k^\pm along the path $\Gamma(0, 0) \rightarrow M(\pi/2, \pi/2) \rightarrow Y(0, \pi) \rightarrow \Gamma$. Fine band splittings on the reduced zone boundary are magnified in the inset. (f) Fine structure of $\tilde{N}_0(\omega)$ around $\tilde{\omega} \sim 0.2$, detected with higher numerical resolution.

only in the electron ($\omega > 0$) side due to the matrix element effect [L_k^- vanishes at $(\pi/2, \pi/2)$]. It is naturally expected that this resonant scattering may open a gap in the fermion excitation spectrum if we go beyond the perturbative scheme. This point can be confirmed through the exact treatment under the uniform \mathcal{V} approximation shown below.

(II) *Uniform approximation.*—Next we consider the case of uniform $\mathcal{V} = (\mathcal{V}_x, \mathcal{V}_y)$ which may locally capture the effects of the circulating $\mathcal{V}(\mathbf{r})$. In this case, we exactly diagonalize the fermion Hamiltonian. The LDOS on the bonds is written in a form $N(\omega)/x\alpha^2 = \tilde{N}_0(\omega) \pm \delta\tilde{N}(\omega)$, where \pm signs alternate from bond to bond. As was inferred from the perturbative analysis, the unit cell doubling splits the one-particle spectrum into two branches [see Fig. 3(e)], $\pm E_k^+$ and $\pm E_k^-$.

In Fig. 3(d), we show the profile of $\tilde{N}_0(\omega)$ and $\tilde{N}_0(\omega) \pm \delta\tilde{N}(\omega)$ for $\mathcal{V} = (-0.1, 0)$, the direction and strength of which correspond to $\mathcal{V}(\mathbf{r})$ around the points B, D and A, C in Fig. 3(a), respectively. We used the same parameter set as in the case of Fig. 3(a). We see that the staggered modulation profile, $\tilde{N}_0(\omega) \pm \delta\tilde{N}(\omega)$, is in remarkable agreement with that obtained by the perturbative analysis. The structures correspond to van Hove singularities associated with the gap opening on the reduced zone boundary, as shown in Fig. 3(e). However, a striking dif-

ference is that the dip structure around $\tilde{\omega} = 0.2$ appears even in the uniform counterpart $\tilde{N}_0(\omega)$. This suggests that in reality the dip structure may be detected not only on the bonds but also at sites. In Fig. 3(d), due to numerical resolution [320×320 mesh of the Brillouin zone] we resolve structures around $\tilde{\omega} = \pm 0.2$ and $\tilde{\omega} = 0.26$. As indicated in Fig. 3(e), there are fine band splittings on the reduced zone boundary leading to van Hove singularities at $\tilde{\omega} = 0.186, 0.216, 0.229$, and 0.265 . The corresponding fine structure in $\tilde{N}_0(\omega)$ could be detected with much higher numerical resolution [720×720 mesh of the Brillouin zone], as shown in Fig. 3(f).

We note that, in both approximations, the modulated structure in the LDOS is predominant on the particle side ($\omega > 0$). We can understand this asymmetry by first turning off the superconductivity and considering the effect of unit cell doubling. Since we are doping with holes, the gaps being opened by the unit cell doubling are on the empty side of the Fermi surface. Matrix element effects preserve this particle-hole asymmetry even after we turn on the superconductivity.

Combining the results obtained through the gradient expansion and the uniform \mathcal{V} approximation, we may reasonably say that the signature of the unit cell doubling may be most prominently detected through the characteristic dip structure inside the V-shaped profile. The structure predicted here is very specific and its observation will be a strong confirmation of the SU(2) vortex model.

J. K. is supported by a Monbusho Grant for overseas research. P. A. L. and X. G. W. acknowledge support by NSF under the MRSEL Program DMR 98-08491. X. G. W. also acknowledges support by NSF Grant No. DMR 97-14198.

*On leave from Department of Theoretical Studies, Institute for Molecular Science, Okazaki 444-8585, Japan.

- [1] Ch. Renner, B. Revaz, K. Kadowaki, I. Maggio-Aprile, and O. Fischer, Phys. Rev. Lett. **80**, 3606 (1998).
- [2] S. H. Pan, E. W. Hudson, A. K. Gupta, K.-W. Ng, H. Eisaki, S. Uchida, and J. C. Davis, Phys. Rev. Lett. **85**, 1536 (2000).
- [3] N. Nagaosa and P. A. Lee, Phys. Rev. B **45**, 966 (1992).
- [4] S. Sachdev, Phys. Rev. B **45**, 389 (1992).
- [5] M. Franz and Z. Tešanović, Phys. Rev. B **63**, 064516 (2001).
- [6] X. G. Wen and P. A. Lee, Phys. Rev. Lett. **76**, 503 (1996).
- [7] P. A. Lee, N. Nagaosa, T. K. Ng, and X. G. Wen, Phys. Rev. B **57**, 6003 (1998).
- [8] P. A. Lee and X.-G. Wen, cond-mat/0008419.
- [9] D. A. Ivanov, P. A. Lee, and X.-G. Wen, Phys. Rev. Lett. **84**, 3958 (2000).
- [10] P. W. Leung, Phys. Rev. B **62**, 6112 (2000).
- [11] J. H. Han, Q.-H. Wang, and D.-H. Lee, cond-mat/0012450.
- [12] Q.-H. Wang, J. H. Han, and D.-H. Lee, cond-mat/0102048.
- [13] I. Affleck and J. B. Marston, Phys. Rev. B **37**, 3774 (1988); T. Hsu, J. B. Marston, and I. Affleck, Phys. Rev. B **43**, 2866 (1991).
- [14] M. R. Norman *et al.*, Nature (London) **392**, 1571 (1998).